Tunable magnetoresistance in thin-film graphite field-effect transistor by gate voltage

Toshihiro Taen,* Kazuhito Uchida, and Toshihito Osada
The Institute for Solid State Physics, The University of Tokyo, Kashiwa, Chiba 277-8581, Japan

Woun Kang
Department of Physics, Ewha Womans University, Seoul 03760, Korea

(Received 19 July 2018; published 23 October 2018)

Magnetic-field-induced semimetal-insulator phase transition in graphite has regained attention, although its mechanism is not fully understood. Recently, a study performed under the pulsed magnetic field discovered that this phase transition depends on thickness even in a relatively thick system of the order of 100 nm and suggested that the electronic state in the insulating phase has an order along the stacking direction. Here we report the thickness dependence observed under dc magnetic fields, which nicely reproduces the previous results obtained under the pulsed magnetic field. In order to look into the critical condition to control the phase transition, the effect of electrostatic gating is also studied in a field-effect transistor structure since it will introduce a spatial modulation along the stacking direction. Magnetoresistance, measured up to 35 T, is prominently enhanced by the gate voltage in spite of the fact that the underlying electronic state is not largely changed owing to the charge-screening effect. On the other hand, the critical magnetic field of the semimetal-insulator transition is found to be insensitive to gate voltages, whereas its thickness dependence is fairly confirmed. By applying positive gate voltages, a prominent oscillation pattern, periodic in magnetic field, becomes apparent, the origin of which is not clear at this stage. Although electrostatic control of the phase transition is not realized in this study, the findings of gate-voltage tunability will help determine the electronic state in the quantum limit in graphite.

DOI: 10.1103/PhysRevB.98.155136

I. INTRODUCTION

A number of studies on topological semimetals, such as Weyl and Dirac semimetals [1–4], have revived interest in the electronic properties in the quantum limit [5–8]. In these materials, owing to their low carrier density and small effective mass, the system easily enters the quantum limit by applying moderate magnetic fields [5,6,9,10]. Graphite is one of the prototypical materials for investigating the electronic properties in the quantum limit [11–42], although it is a topologically trivial material. The Landau subband structure under magnetic fields as large as $B \simeq 30$ T is the so-called quasiquantum limit, where all carriers populate only four quasi-one-dimensional Landau subbands at the Fermi level. The calculated Landau subband structure based on the Slonczewski-Weiss-McClure model [43–45] is demonstrated in Fig. 1(a). Since graphite has two energetically equivalent valleys along the H-K-H and H'-K'-H' lines [Fig. 1(b)], those subbands are also valley degenerate. One of the notable features showing up at this condition is a semimetal-insulator transition. The electronic state in the insulating phase is proposed to be an exotic density-wave state [26,31,38–41,46]. For example, in the valley-density-wave state, each valley forms a charge-density wave (CDW), but the waves are antiphase to each other [38], although this has been difficult to verify experimentally. The presence of the thickness dependence of the phase transition, recently discovered under the pulsed magnetic field [36], implies that an ordered state evolves along the stacking (c-axis) direction. Moreover, a deviation from the bulk properties was observed even in a relatively thick sample of around 200 nm (≈300 unit cells). The density-wave model combined with a quantum size effect is successful in qualitatively reproducing the experimental results; the phase transition line shifts towards higher magnetic fields, and its temperature dependence becomes small with decreasing thickness. These features are attributed to the discrete wave number and sparse energy spacing, respectively, in accordance with decreasing thickness. Although the experiment in Ref. [36] was carefully designed to avoid the eddy-current-heating problem in the pulsed magnetic field by using microcrystals, it is desirable to confirm the thickness dependence in the dc magnetic field. In this study, as a first step, we report the reproducibility of the thickness dependence under dc magnetic field.

Moreover, as the thickness dependence is present, it is interesting to introduce a spatial modulation along the stacking direction. The structure of a field-effect transistor (FET) can realize it. A standard semiconductor FET forms a conductive channel at the interface on the substrate by concentrating doped carriers under gate voltage. However, in the case of a semimetallic graphite FET with a thickness of the order of $d \simeq 100$ nm, the charge-screening effect should be taken into account. Suppose that, by making the situation simpler, the spatially varied electrostatic potential V_{es} (i.e., with band bending) divides the system into two parts: the interface and

*taen@issp.u-tokyo.ac.jp

 ©2018 American Physical Society

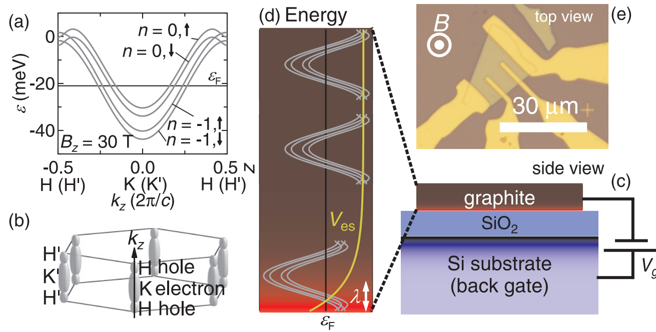

FIG. 1. (a) Landau subband structure under $B = 30$ T along the k_z axis ($k_z||c$). The so-called quasiquantum limit (only four subbands reside at the Fermi level ε_F) is realized. The calculation is based on the Slonczewski-Weiss-McClure model [43–45]. (b) Schematic view of the Brillouin zone and Fermi surfaces at $B = 0$ in graphite. At the zone corners of the H-K-H and H'-K'-H' lines, electron and hole pockets are formed. The size of Fermi surfaces is exaggerated. (c) Schematic view of the FET structure (side view). Thin-film graphite is placed on a Si/SiO$_2$ substrate, which functions as a back-gate electrode in applying gate voltage V_g. (d) Schematic view of band bending and carrier doping under gate voltage V_g. Owing to the screening effect, the electrostatic potential V_{es} bends at the interface in the range of screening length λ, and most of the doped carriers concentrate on the interface (bright region). (e) Optical microscopy image of a 70-nm-thick sample (top view) after fabrication of the electrode. Magnetic field B is applied perpendicular to the plate.

bulk parts. The interface part, characterized by the thickness of a screening length λ, hosts most of the doped carriers, and the bulk part, with a thickness of $d - \lambda$, keeps the electronic state the same as the original (nondoped) state [schematically drawn in Figs. 1(c) and 1(d)]. A previous study supports such a model [47], where the charge distribution and the potential in such a system were self-consistently calculated and it was concluded that most doped carriers concentrate on a few layers at the interface but part of them penetrates into the bulk part in association with oscillations. A short λ was experimentally confirmed in dual-gated few-layer graphene [48]. If an effective thickness $d - \lambda$ can be controlled in such a way, the phase transition can be controlled in an electrostatic way, leading to deep insight into the electronic state of the insulator phase. On the other hand, the carrier doping possibly shifts the critical magnetic field of the phase transition in an ambipolar way, as discussed for neutron-irradiated graphite, in which hole carriers were doped [19]. In the FET structure, since the electrostatic doping introduces the nonuniformity, the effect of the gate voltage is not clear. In this study, by observing magnetotransport properties, we clarify the effect of gate voltage on the electronic state under the magnetic fields in a thin-film graphite FET system. By analyzing Shubnikov–de Haas (SdH) oscillations and the magnitude of the magnetoresistance (MR), band bending and carrier doping are qualitatively evaluated. The dependence of the phase transition over a wide range of gate voltage is investigated by applying high magnetic field up to 35 T. The ability of the phase-transition shift by electrostatic gating is discussed by considering the strong charge-screening effect.

II. EXPERIMENTAL METHODS

Thin-film graphite with an FET structure was fabricated on a heavily doped silicon wafer with a 300-nm-thick dielectric topmost layer formed by thermal oxidation, which functions as a back-gate electrode [Fig. 1(c)]. Mechanically exfoliated Kish graphite microcrystals were transferred onto the substrate. Atomic-force microscopy was used to choose samples with a flat surface and to measure their thickness. The typical dimensions of the samples were $30\times30\times0.1$ μm^3 [Fig. 1(e)]. In this paper, samples with thicknesses $d = 70$ and 178 nm are studied. Electrical contacts for in-plane resistance measurements were formed by thermally evaporating gold on a $Ni_{0.8}Cr_{0.2}$ sticking layer after electron-beam lithography. High magnetic fields B were generated in a 35-T resistive magnet at the National High Magnetic Field Laboratory. The dc electrical resistance R was measured by reversing a constant current under B along the c axis (perpendicular to the plate) at low temperature T down to 0.35 K in a ^{3}He refrigerator. The static gate voltage V_g was applied within the range of -80 V $\leqslant V_g \leqslant +80$ V.

III. RESULTS

Typical in-plane resistance as a function of magnetic field in thin-film graphite for various gate voltages is shown in Fig. 2(a). Here only the results for 70-nm-thick samples are shown, and those for the 178-nm-thick sample are given in Appendix A. The overall trend is similar for all gate voltages; it shows a sizable MR up to $B \approx 25$ T, superimposed with SdH oscillations below $B \approx 8$ T, and a semimetal-insulator transition occurs around $B \equiv B_c \approx 30$ T. In addition, gate-voltage-dependent features are also identified, although the effect of the gate voltage is different in different magnetic-field regions, as color-coded in Fig. 2(a).

In the first region below $B \approx 8$ T, the SdH oscillations under gate voltage appear at the same magnetic fields as those without gate voltage ($V_g = 0$), but the amplitude of the SdH oscillations becomes larger with increasing V_g. Since the oscillations reflect the evolution of the Landau subband structure, this gate-voltage independence indicates that the electronic structure of the bulk part is unchanged even under a large gate voltage.

In the second region between $\approx$8 T and B_c, it is clear that MR strongly depends on gate voltage. These features are clearly shown in Fig. 2(g), where the gate-voltage dependence of MR is replotted from Fig. 2(a) at several magnetic fields, indicated by vertical dashed lines. This is in stark contrast to the gate-voltage dependence under zero magnetic field. It is noteworthy that an oscillatory behavior is found only under positive gate voltages, which will be elaborated on later.

The third region is above $B = B_c$. Here we define B_c by the cross point of linear fitting curves below and above the kink structure at $B \approx 30$ T. In contrast to the thickness dependence, the gate-voltage dependence of B_c is negligible, as shown in the phase diagram (Fig. 3). The phase boundary of the bulk system in Ref. [19] is also shown. It is evident that the phase boundary shifts towards higher magnetic fields with reducing thickness. This result is the first confirmation of the thickness-dependent B_c under the dc magnetic field and consistent with

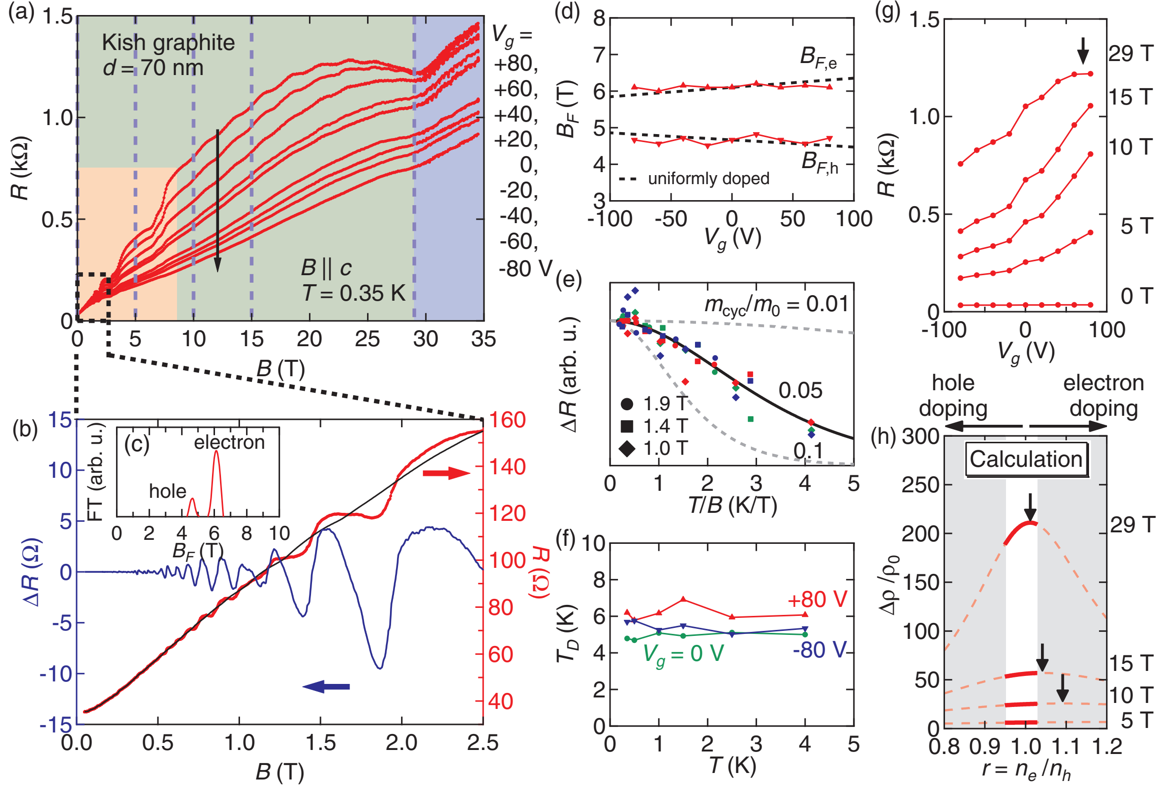

FIG. 2. (a) In-plane resistance R of 70-nm-thick graphite as a function of out-of-plane magnetic field B at $T = 0.35$ K for gate voltages $V_g = +80, +60, +40, +20, 0, -20, -40, -60$, and -80 V, from top to bottom. Gate-voltage dependence is different in different colored regions. In addition, oscillatory behavior periodic in B is observed between 10 T and B_c but only under positive gate voltages. (b) In-plane resistance R, smoothed background $R_{\rm bg}$, and Shubnikov–de Haas component $\Delta R = R - R_{\rm bg}$ for $B \leqslant 2.5$ T. (c) Fourier transform spectrum of the low magnetic field $\Delta R(1/B)$. The frequencies of hole and electron pockets are $B_{F,h} = 4.7$ T and $B_{F,e} = 6.1$ T, respectively. (d) Gate-voltage dependence of $B_{F,h}$ and $B_{F,e}$. The expected lines in the uniformly doped model are also shown with dashed lines. (e) T/B dependence of ΔR of Shubnikov–de Haas oscillations at some magnetic fields. Red, green, and blue symbols indicate data at gate voltages $V_g = +80$, 0, and -80 V, respectively, as shown in (f). ΔR for different magnetic fields and gate voltages are scaled. All the data can fit reasonably well on a theoretical line of $m_{\rm cyc}/m_0 = 0.05$. (f) Dingle temperature T_D at gate voltages of $V_g = +80$, 0, and -80 V. T_D is weakly dependent on gate voltages. (g) Gate-voltage dependence of MR at several magnetic fields indicated by vertical dashed lines in (a). Gate-voltage dependence becomes more pronounced at high magnetic field and shows a maximum at $B = 29$ T, indicated by an arrow. (h) Two-carrier-model calculation of the MR as a function of the ratio of electron to hole carrier densities, shown in Eq. (1) with $m = \mu_e/\mu_h = 0.2$ and $\overline{\mu} = \sqrt{\mu_e \mu_h} = 0.5$ T^{-1}. The peak position under each magnetic field is indicated by an arrow. At high magnetic fields, the peak approaches $r = 1$, while it deviates for lower magnetic fields when $m \neq 1$. Only the bright region around $r = 1$ is expected to be observed in the present experiment [(g)]. In (g) and (h), right and left directions along the horizontal axis correspond to electron and hole doping, respectively.

the findings under the pulsed magnetic field in Ref. [36]. This coincidence proves that the minimization of the eddy current heating using microcrystal graphite worked under the pulsed magnetic field [36]. By contrast, the gate-voltage dependence of B_c is negligible.

IV. DISCUSSION

The gate-voltage dependence is weak in the first ($B < 8$ T) and third ($B \geqslant B_c$) regions, whereas it is strong in the second (8 T $\leqslant B < B_c$) region. In order to consider the effects of gate voltage on the underlying band structure, the oscillatory component ΔR is extracted by subtracting smoothed (moving window average) background data $R_{\rm bg}$ from raw data R, as shown in Fig. 2(b). As discussed by Schneider *et al.* [49], Fermi energy can be regarded to be constant only at low magnetic fields. Hence, the frequency analyses are performed below 2 T.

Fourier transformation of the oscillatory component $\Delta R \equiv R - R_{\rm bg}$ as a function of the inverse of magnetic field $(1/B)$ produces two peaks at $B_{F,h} = 4.7$ T and $B_{F,e} = 6.1$ T, as shown in Fig. 2(c). As is well known in bulk graphite, these two frequencies are attributable to the hole and electron Fermi pockets, respectively. Both frequencies are almost independent of the gate voltage, as can be seen in Fig. 2(d). This result is in stark contrast to what is observed in 35-nm-thick highly oriented pyrolytic graphite (HOPG), where SdH oscillations are different from those in the bulk system even at $V_g = 0$ and depend on the gate voltage in spite of the presence of the screening effect [37]. The weak gate-voltage dependence of the SdH frequencies in our study reflects the strong screening effect, which supports our expectation of the introduction of spatial modulation along the stacking direction. Namely, doped carriers concentrate at the interface, and the electronic structure in the bulk part is largely unchanged. The resultant band bending is schematically illustrated in Fig. 1(d). In fact,

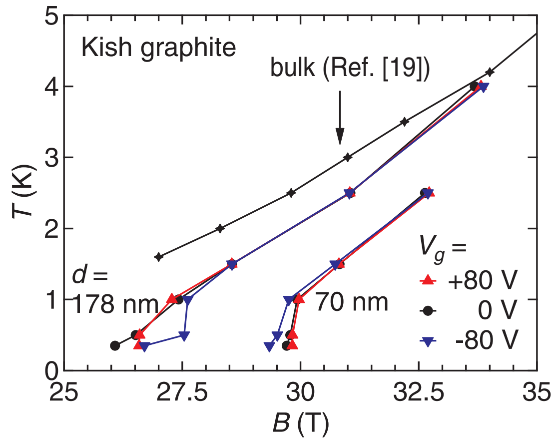

FIG. 3. Temperature-magnetic-field phase diagram of 178- and 70-nm-thick graphite samples under several gate voltages. The phase boundary in the bulk system [19] is also shown. In contrast to the thickness dependence reported in Ref. [36], gate-voltage dependence is negligible.

the screening length λ of multilayer graphene was reported to be a few layers [47,48,50], which is a fingerprint of the strong screening effect. Note that there is no sign of interface-derived SdH oscillations. This suggests that transport properties are dominated by the bulk region.

Meanwhile, the gate voltage strongly affects the magnitude of MR. According to the semiclassical two-carrier model, MR is expressed as

$$\frac{\Delta\rho}{\rho_0} = \frac{r^{-1}(1+m)^2(\overline{\mu}B)^2}{(r^{-1}+m)^2 + m(r^{-1}-1)^2(\overline{\mu}B)^2}, \quad (1)$$

where $r = n_e/n_h$ is the ratio of electron (n_e) to hole (n_h) carrier densities, $m = \mu_e/\mu_h$ is the ratio of electron (μ_e) to hole (μ_h) mobilities, and $\overline{\mu} = \sqrt{\mu_e\mu_h}$ is the geometrical mean of the electron and hole mobilities. According to Eq. (1), an imbalance between electron and hole carrier densities (deviation from $r = 1$) or a change in the averaged mobility $\overline{\mu}$ significantly affects the magnitude of MR. In order to identify the origin of the gate-voltage dependence of MR in terms of r and $\overline{\mu}$, the amplitude of SdH oscillations in ΔR is analyzed below.

According to the Lifshitz-Kosevich theory, the temperature dependence of the SdH oscillation amplitude becomes larger as the cyclotron mass $m_{\rm cyc}$ increases, and the magnetic-field dependence is affected by the scattering rate τ^{-1}, which is proportional to the Dingle temperature as $T_D = \hbar/2\pi k_B\tau$. By using the amplitudes at $B = 1.9$, 1.4, and 1.0 T, the gate-voltage-independent cyclotron mass is found to be $m_{\rm cyc}/m_0 = 0.05$ [Fig. 2(e)], where m_0 is the free-electron rest mass. The Dingle temperature is weakly dependent on the gate voltage within the range of $T_D \approx 4$–6 K [Fig. 2(f)]. Note that the oscillations at these magnetic fields contain both electron and hole components, so that their averaged characteristic would be observed. Such insensitivity of $m_{\rm cyc}$ and T_D to the gate voltage suggests that the average mobility $\overline{\mu}$ is not varied much by the gate voltage.

Hence, we need to revisit the possibility of the variation of carrier densities. The strength of the screening effect determines whether the carrier doping effect is truly negligible in the bulk part. In a uniformly doped model, where the screening effect is supposed to be absent and doped carriers are uniformly distributed in the system, the expected dependence of the SdH frequency on V_g is shown by the dashed lines in Fig. 2(d). (The details of this model are explained in Appendix B.) Although the gate-voltage dependence of our experimental result is smaller than that in the uniformly doped model, the difference between them is not very large. This means that a finite amount of doping in the bulk part cannot be denied, although the majority of the doped carriers concentrate on the interface. This situation was theoretically proposed in Ref. [47]. If we assume this small carrier doping in the bulk part, the gate-voltage dependence of MR is qualitatively reproduced by the two-carrier model as follows.

The gate-voltage dependence of in-plane resistance at a constant magnetic field is shown in Fig. 2(g). In the absence of magnetic field, the gate-voltage dependence of the resistance is negligibly small but becomes strong under high magnetic fields and has a peak at positive V_g (indicated by an arrow) under a very high magnetic field of $B = 29$ T. The peak position approaches $V_g = 0$ by increasing magnetic fields. The same trend is observed in the 178-nm-thick sample (Appendix A).

In the case of monolayer or bilayer graphene, such a peak structure reflects an energy-dependent density of states $D(E)$, and the peak appears when the chemical potential is tuned to the Dirac point. However, this interpretation does not work in the present thin-film graphite system since the overall chemical potential cannot be controlled owing to the screening effect. In fact, the gate-voltage dependence is absent at $B = 0$. Therefore, this peak structure is not derived from the carrier doping in the interface part but originates from the bulk part, as is the case for SdH oscillations.

Instead, the two-carrier model, shown in Eq. (1), is preferable. Although such a semiclassical model is not strictly adequate in the quasiquantum limit, the model is successful in qualitatively describing the behavior in the case of a Weyl semimetal [10]. An example of the calculated $\Delta\rho/\rho_0$ as a function of r for the case of $m = 0.2$ and $\overline{\mu} = 0.5$ T^{-1} is illustrated with solid lines in Fig. 2(h). The calculated results succeed in qualitatively reproducing the experimental results in Fig. 2(g). An unsaturated MR for $B \to \infty$ is realized only when the carrier compensation $n_e = n_h$ is satisfied, which means that $\Delta\rho/\rho_0(r)$ has a maximum at $r = 1$ under high enough magnetic field. However, $\Delta\rho/\rho_0(r)$ peaks at $r \neq 1$ for lower magnetic fields when $m \neq 1$, as can be seen in the case of $B = 5$ and 10 T in Fig. 2(h). Our experimental results imply that the MR peaks at V_g higher than the range of the measurement at lower magnetic fields, which corresponds to $m < 1$ in Eq. (1).

As a result, the observed gate-voltage dependence of MR is consistent with a small amount of carrier doping in the two-carrier model. As discussed above, this interpretation does not conflict with the gate-voltage dependence of SdH frequencies since a small amount of carrier doping possibly exists in the bulk region. Although the observed behavior is not fully explained by this model, for example, negative differential MR at $B \approx 23$–29 T under positive gate voltage and the absence of quantitative agreement, the trend of the gate voltage dependence is qualitatively reproduced by the simple two-carrier model.

As seen in the first and second regions, the effect of applying gate voltage is carrier doping and band bending along the stacking direction. These two effects might shift the semimetal-insulator phase transition in the following ways. If the band-bending effect dominates, the phase boundary shifts towards higher magnetic field owing to the reduced effective thickness $d - \lambda$, as in the case of the thickness-dependent shift in Ref. [36]. If the carrier-doping effect affects the phase transition, on the other hand, the phase transition line is expected to be shifted to both higher and lower magnetic fields depending on the doped carrier type. Suppose that the Landau subbands at a given magnetic field B_a close to B_c are doped by holes as a manner of rigid-band shift. If we focus on one of the subbands [$n = 0, \uparrow$; see Fig. 1(a)], the doped subband is similar to the nondoped one at magnetic field higher than B_a. As a result, the phase transition is expected to shift to higher magnetic field with the introduction of the hole carrier. Part of the shift observed in neutron-irradiated graphite is believed to be due to hole doping [19,23,24].

However, the shift of the critical magnetic field is found to be negligibly small in the present study in both the 70- and 178-nm-thick samples, as shown in Fig. 3. The absence of the gate-voltage effect on the phase transition can be explained as follows. A short λ means that the effective thickness $d - \lambda$ is not changed much, resulting in the negligible reduction of effective thickness. In addition, a small amount of doped carrier density in the bulk region is not enough to shift the phase boundary. In the uniformly doped model, the doped carrier density is on the order of 10^{16} cm^{-3} at $V_g = 100$ V. In reality, however, the doping effect is largely reduced by the screening effect in the bulk region. In fact, in the case of neutron irradiation experiments, the amount of carrier doping $n_h - n_e = 3\times10^{16}$ cm^{-3} is necessary for significant effect, which will not be achieved in the current solid-gate FET system owing to the screening effect. It should be noted that there is room for further research into tuning the phase transition by stronger gating or in a thinner sample whose thickness is comparable to λ.

Finally, an intriguing phenomenon observed in the second region should be pointed out. Oscillatory behavior at $10\ \mathrm{T} \leqslant B \leqslant B_c$ was discovered. An example is represented in Fig. 4(a). The observed oscillations between 10 T and B_c were highly reproducible and more prominent at positive gate voltages. The amplitude is systematically changed by gate voltages, as shown in the inset of Fig. 4(b). In order to determine whether the observed oscillations are SdH oscillations, a smoothed background R_{bg} is subtracted from the raw data R and $\Delta R = R - R_{\mathrm{bg}}$ is shown as a function of magnetic field B in Fig. 4(a), It is clear that ΔR is periodic in B, instead of $1/B$ known in SdH oscillations, demonstrating that the origin is different from that of SdH oscillations. A single period $\Delta B \approx 2.5$ T is found which is stable for varying gate voltages and temperatures but different from that in the other sample ($\Delta B \approx 1$ T in the 178-nm-thick sample). We note that these two samples are mounted and measured at the same time, so that an artifact, such as mechanical oscillation of the system, is excluded from the origin. On the other hand, the amplitude of the oscillations is almost constant at $10\ \mathrm{T} \leqslant B \leqslant B_c$ and monotonically shrinks with reducing gate voltage, as shown in Fig. 4(b). This strong gate-voltage dependence is in contrast to noiselike features found above $B \approx B_c$, which is similar to the behavior reported by Timp *et al.* [17]. Note that they found oscillatory behavior periodic in B only above B_c and attributed it to spin-orbit splitting of π bands in graphite or in-plane modulation derived from CDW.

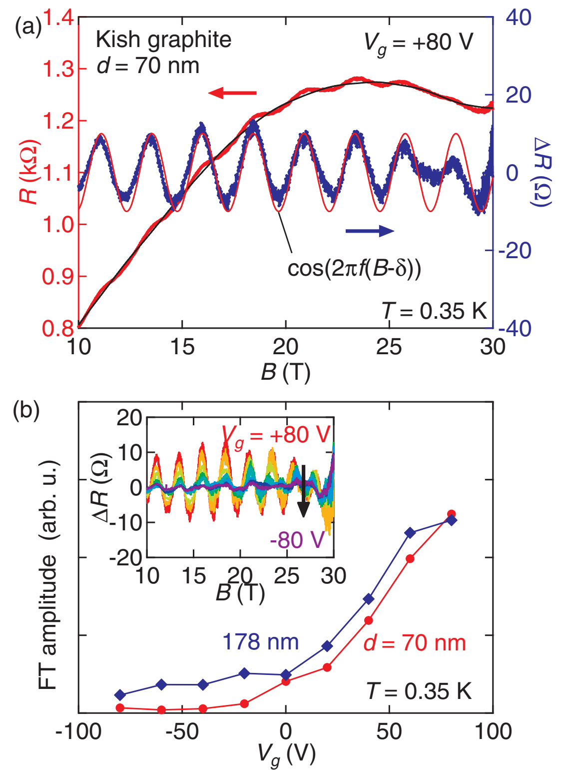

FIG. 4. (a) In-plane resistance R, smoothed background R_{bg}, and the oscillatory component $\Delta R = R - R_{\mathrm{bg}}$ as a function of magnetic field B. ΔR is in reasonably good agreement with $\cos[2\pi f(B - \delta)]$, where $f \approx (2.5\ \mathrm{T})^{-1}$ is the frequency and δ is a phase factor. (b) Gate-voltage dependence of the oscillation amplitude in the 70- and 178-nm-thick samples. Both systems show finite amplitude at $V_g > 0$. Inset: ΔR as a function of magnetic field B at various gate voltage $V_g = +80, +60, +40, +20, 0, -20, -40, -60$, and -80 V in the 70-nm-thick sample. The amplitude of Fourier transform is depicted in the main panel.

An oscillatory behavior periodic in B is normally associated with the Aharanov-Bohm effect. By assigning one cycle of oscillation with a flux quantum ϕ_0, the effective area of interference $S = \phi_0/\Delta B$ is 170 nm^2 for the 70-nm-thick sample and 410 nm^2 for the 178-nm-thick sample. In-plane carrier modulation is one of the candidates to give this S. Fukuyama discussed the in-plane CDW instability under high magnetic field [51], but this oscillation starts from 10 T, far below B_c. Recently, very similar behavior was reported in HOPG bulk crystals [52], where multiple periods with $\Delta B = 1$–4 T are observed, and those oscillations are almost quenched by raising the temperature to 4.2 K. The amplitude of the conductance oscillations was found to be $\delta G = 1/R - 1/R_{\mathrm{bg}} \simeq 2 - 3\ e^2/h$, which is relatively close to our observation ($\delta G \simeq 0.1 - 0.2\ e^2/h$ at $T = 0.35$ K). By contrast, in the present thin film of Kish graphite, the oscillations are composed of a single period, and the temperature dependence

of the amplitude is absent below 4 K. Rischau *et al.* suggested that its origin is attributable to the moiré superlattice formed at the interface between two crystalline regions [52]. In fact, the importance of such an interface for the transport property is discussed in Ref. [53]. However, in contrast to HOPG, such a moiré pattern would be absent in the case of Kish graphite owing to the difference in crystal perfectness. In addition, if the mechanism of the moiré pattern were realized even in Kish graphite, several periods of ΔB should be observed, which conflicts with our observation. We leave this as an open problem since unveiling the origin of this behavior is beyond the scope of this paper. Since this feature appears just after the quasiquantum limit is realized, it might originate from the quantum effect.

V. CONCLUSION

In conclusion, by measuring magnetotransport properties under dc magnetic field in FET-structured graphite with thicknesses of 70 and 178 nm, we confirmed that the thickness-dependent phase transition is evident. In addition, a spatial modulation along the stacking direction was successfully introduced in thin-film graphite of the order of 100 nm. The gate-voltage dependence of SdH oscillations is small and is ascribed to the strong screening effect. The bulk part dominates the transport properties. By contrast, the magnitude of MR is highly tunable with gate voltage. The nonmonotonic gate-voltage dependence of MR is qualitatively reproduced by the conventional two-carrier model. These results indicate a small amount of charge doping even in the bulk region in spite of the screening effect. The semimetal-insulator transition is expected to be affected by the reduction of effective thickness or by the carrier doping effect, but neither of them is observed in the current solid-gate FET system. This robustness possibly provides the lower limit of the key ingredient for the phase transition. In addition, an oscillation, periodic in magnetic field, was observed especially under positive gate voltages in the range of the quasiquantum limit, the origin of which is an open question. Although the shift of the semimetal-insulator transition is not significant in our samples, a thin-film FET structure opens up the possibility of the continuous variation of the critical condition for the phase transition by stronger gating or by using thinner films, which will clarify the evolution of the electronic state in the quantum limit.

ACKNOWLEDGMENTS

The authors acknowledge Dr. E S. Choi for technical support and discussions. The authors also thank to Dr. B. Fauqué for fruitful discussions. A portion of this work was performed at the National High Magnetic Field Laboratory, which is supported by National Science Foundation Cooperative Agreement No. DMR-1157490 and the state of Florida. This work was partially supported by JSPS KAKENHI Grants No. JP15K21722, No. JP25107003, No. JP16H03999, and No. JP16K17739. W.K. was also supported by Basic Science Research Program through the National Research Foundation of Korea (NRF) funded by the Ministry of Education (No. 2018R1D1A1B07050087 and No. 2018R1A6A1A03025340).

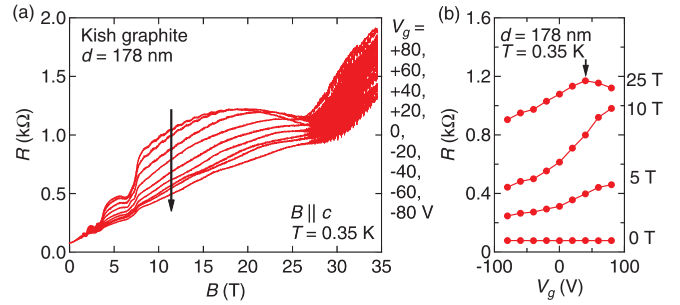

FIG. 5. (a) In-plane resistance of the 178-nm-thick sample as a function of magnetic field at $T = 0.35$ K under various gate voltages. (b) Gate-voltage dependence of in-plane resistance under several magnetic fields at $T = 0.35$ K in the 178-nm-thick sample. The peak at $B = 25$ T is indicated by an arrow.

APPENDIX A: MAGNETORESISTANCE IN 178-NM-THICK SAMPLE

The trend discussed for the 70-nm-thick sample (in the main text) is observed also in the 178-nm-thick sample. In-plane resistance as a function of magnetic field is exemplified in Fig. 5(a), which is similar to that in the 70-nm-thick sample [Fig. 2(a)]. The obtained plots for cyclotron mass and Dingle temperature are also similar to those for the 70-nm-thick system [Figs. 2(d), 2(e), and 2(f)]. As can be seen in Fig. 5(b), the gate-voltage dependence of in-plane resistance is clear. This system also shows a maximum under high magnetic fields, as marked with an arrow.

APPENDIX B: UNIFORMLY DOPED MODEL

If the screening effect is absent, carriers will be uniformly doped, which should be observed in SdH oscillations. A single-carrier system is assumed for simplicity. The observed frequency in SdH oscillations is three-dimensional, but the number of carriers by means of electrostatic doping in the FET structure should be counted by areal density. Since carriers are assumed to be doped homogeneously in this model, the areal density of doped carriers n'_{2D} should be treated as the volume density of doped carriers $n'_{3D} = n'_{2D}/d$. The total three-dimensional carrier density is written as $\overline{n_{3D}} = n_{3D} + n'_{3D}$, where n_{3D} is the volume density of carriers in a nondoped system. By uniform doping, the volume in reciprocal space enclosed by Fermi surfaces should change, and the Fermi wave vector k_F also changes as $\overline{k_F} = \alpha k_F$, which results in the change in carrier density $(n_{3D} \rightarrow \overline{n_{3D}} = \alpha^3 n_{3D})$ and extremal cross section $(S_F \rightarrow \overline{S_F} = \alpha^2 S_F)$. The enhancement factor α is obtained as $\alpha = (1 + n'_{2D}/n_{3D}d)^{1/3}$ by solving the relation $\overline{n_{3D}} = n_{3D} + n'_{3D} = \alpha^3 n_{3D}$. Since the frequency of SdH oscillations B_F is proportional to S_F, the SdH frequency under gate voltage $\overline{B_F}$ is expressed as

$$\overline{B_F} = \left(1 + \frac{n'_{2D}}{n_{3D}d}\right)^{2/3} B_F, \quad \text{(B1)}$$

where B_F is the SdH frequency in the nondoped system. By substituting typical values, $n_{3D} = 8\times10^{18}$ cm^{-3}, $d = 70$ nm, and $n'_{2D} = 7\times10^{12}$ cm^{-2} at $V_g = 100$ V, a factor of the change in frequency is evaluated as $\overline{B_F}/B_F = 1.08$, which is plotted in Fig. 2(d).

[1] Z. K. Liu, B. Zhou, Y. Zhang, Z. J. Wang, H. M. Weng, D. Prabhakaran, S.-K. Mo, Z. X. Shen, Z. Fang, X. Dai, Z. Hussain, and Y. L. Chen, Science **343**, 864 (2014).
[2] M. Neupane, S.-Y. Xu, R. Sankar, N. Alidoust, G. Bian, C. Liu, I. Belopolski, T.-R. Chang, H.-T. Jeng, H. Lin, A. Bansil, F. Chou, and M. Z. Hasan, Nat. Commun. **5**, 3786 (2014).
[3] S.-M. Huang, S.-Y. Xu, I. Belopolski, C.-C. Lee, G. Chang, B. Wang, N. Alidoust, G. Bian, M. Neupane, C. Zhang, S. Jia, A. Bansil, H. Lin, and M. Z. Hasan, Nat. Commun. **6**, 7373 (2015).
[4] H. Weng, C. Fang, Z. Fang, B. A. Bernevig, and X. Dai, Phys. Rev. X **5**, 011029 (2015).
[5] P. Kim, J. H. Ryoo, and C.-H. Park, Phys. Rev. Lett. **119**, 266401 (2017).
[6] C.-L. Zhang, S.-Y. Xu, C. M. Wang, Z. Lin, Z. Z. Du, C. Guo, C.-C. Lee, H. Lu, Y. Feng, S.-M. Huang, G. Chang, C.-H. Hsu, H. Liu, H. Lin, L. Li, C. Zhang, J. Zhang, X.-C. Xie, T. Neupert, M. Z. Hasan, H.-Z. Lu, J. Wang, and S. Jia, Nat. Phys. **13**, 979 (2017).
[7] Q. R. Zhang, B. Zeng, D. Rhodes, S. Memaran, T. Besara, R. Sankar, F. Chou, N. Alidoust, S.-Y. Xu, I. Belopolski, M. Z. Hasan, and L. Balicas, arXiv:1705.00920.
[8] C.-L. Zhang, F. Schindler, H. Liu, T.-R. Chang, S.-Y. Xu, G. Chang, W. Hua, H. Jiang, Z. Yuan, J. Sun, H.-T. Jeng, H.-Z. Lu, H. Lin, M. Z. Hasan, X. C. Xie, T. Neupert, and S. Jia, Phys. Rev. B **96**, 165148 (2017).
[9] L. R. Thoutam, Y. L. Wang, Z. L. Xiao, S. Das, A. Luican-Mayer, R. Divan, G. W. Crabtree, and W. K. Kwok, Phys. Rev. Lett. **115**, 046602 (2015).
[10] M. N. Ali, J. Xiong, S. Flynn, J. Tao, Q. D. Gibson, L. M. Schoop, T. Liang, N. Haldolaarachchige, M. Hirschberger, N. P. Ong, and R. J. Cava, Nature (London) **514**, 205 (2014).
[11] S. Tanuma, R. Inada, A. Furukawa, O. Takahashi, Y. Iye, and Y. Onuki, in *Physics in High Magnetic Fields*, edited by S. Chikazumi and N. Miura (Springer, Berlin, 1981), p. 316.
[12] Y. Iye, P. Berglund, and L. McNeil, Solid State Commun. **52**, 975 (1984).
[13] Y. Iye and G. Dresselhaus, Phys. Rev. Lett. **54**, 1182 (1985).
[14] Y. Iye, L. E. McNeil, and G. Dresselhaus, Phys. Rev. B **30**, 7009 (1984).
[15] Y. Iye, C. Murayama, N. Mōri, S. Yomo, J. T. Nicholls, and G. Dresselhaus, Phys. Rev. B **41**, 3249(R) (1990).
[16] Y. Iye, P. M. Tedrow, G. Timp, M. Shayegan, M. S. Dresselhaus, G. Dresselhaus, A. Furukawa, and S. Tanuma, Phys. Rev. B **25**, 5478 (1982).
[17] G. Timp, P. D. Dresselhaus, T. C. Chieu, G. Dresselhaus, and Y. Iye, Phys. Rev. B **28**, 7393 (1983).
[18] H. Yaguchi, Y. Iye, T. Takamasu, and N. Miura, Phys. B (Amsterdam, Neth.) **184**, 332 (1993).
[19] H. Yaguchi, Y. Iye, T. Takamasu, N. Miura, and T. Iwata, J. Phys. Soc. Jpn. **68**, 1300 (1999).
[20] H. Yaguchi, T. Takamasu, Y. Iye, and N. Miura, J. Phys. Soc. Jpn. **68**, 181 (1999).
[21] H. Yaguchi and J. Singleton, Phys. B (Amsterdam, Neth.) **256–258**, 621 (1998).
[22] H. Yaguchi, J. Singleton, and T. Iwata, Phys. B (Amsterdam, Neth.) **298**, 546 (2001).
[23] H. Yaguchi and J. Singleton, J. Phys.: Conf. Ser. **150**, 022099 (2009).
[24] H. Yaguchi and J. Singleton, J. Phys.: Condens. Matter **21**, 344207 (2009).
[25] B. Fauqué, D. LeBoeuf, B. Vignolle, M. Nardone, C. Proust, and K. Behnia, Phys. Rev. Lett. **110**, 266601 (2013).
[26] K. Akiba, A. Miyake, H. Yaguchi, A. Matsuo, K. Kindo, and M. Tokunaga, J. Phys. Soc. Jpn. **84**, 054709 (2015).
[27] H. Ochimizu, T. Takamasu, S. Takeyama, S. Sasaki, and N. Miura, Phys. Rev. B **46**, 1986 (1992).
[28] Y. Kopelevich, B. Raquet, M. Goiran, W. Escoffier, R. R. da Silva, J. C. Medina Pantoja, I. A. Luk'yanchuk, A. Sinchenko, and P. Monceau, Phys. Rev. Lett. **103**, 116802 (2009).
[29] F. Arnold, A. Isidori, E. Kampert, B. Yager, M. Eschrig, and J. Saunders, Phys. Rev. Lett. **119**, 136601 (2017).
[30] S. Uji, J. Brooks, and Y. Iye, Phys. B (Amsterdam, Neth.) **246–247**, 299 (1998).
[31] Z. Zhu, R. D. McDonald, A. Shekhter, B. J. Ramshaw, K. A. Modic, F. F. Balakirev, and N. Harrison, Sci. Rep. **7**, 1733 (2017).
[32] D. V. Khveshchenko, Phys. Rev. Lett. **87**, 206401 (2001).
[33] A. Kumar, J.-M. Poumirol, W. Escoffier, M. Goiran, B. Raquet, and J. C. Pivin, J. Phys.: Condens. Matter **22**, 436004 (2010).
[34] X. Du, S.-W. Tsai, D. L. Maslov, and A. F. Hebard, Phys. Rev. Lett. **94**, 166601 (2005).
[35] E. Jobiliong, J. Park, J. Brooks, and R. Vasic, Curr. Appl. Phys. **7**, 338 (2007).
[36] T. Taen, K. Uchida, and T. Osada, Phys. Rev. B **97**, 115122 (2018).
[37] B. C. Camargo and W. Escoffier, Carbon **139**, 210 (2018).
[38] D. Yoshioka and H. Fukuyama, J. Phys. Soc. Jpn. **50**, 725 (1981).
[39] Y. Takada and H. Goto, J. Phys.: Condens. Matter **10**, 11315 (1998).
[40] K. Takahashi and Y. Takada, Phys. B (Amsterdam, Neth.) **201**, 384 (1994).
[41] K. Sugihara, Phys. Rev. B **29**, 6722 (1984).
[42] D. D. L. Chung, J. Mater. Sci. **37**, 1475 (2002).
[43] J. C. Slonczewski and P. R. Weiss, Phys. Rev. **109**, 272 (1958).
[44] J. W. McClure, Phys. Rev. **119**, 606 (1960).
[45] M. Inoue, J. Phys. Soc. Jpn. **17**, 808 (1962).
[46] Z. Pan, X.-T. Zhang, and R. Shindou, arXiv:1802.10253.
[47] F. Guinea, Phys. Rev. B **75**, 235433 (2007).
[48] H. Miyazaki, S. Odaka, T. Sato, S. Tanaka, H. Goto, A. Kanda, K. Tsukagoshi, Y. Ootuka, and Y. Aoyagi, Appl. Phys. Express **1**, 034007 (2008).
[49] J. M. Schneider, M. Orlita, M. Potemski, and D. K. Maude, Phys. Rev. Lett. **102**, 166403 (2009).
[50] T. Ohta, A. Bostwick, J. L. McChesney, T. Seyller, K. Horn, and E. Rotenberg, Phys. Rev. Lett. **98**, 206802 (2007).
[51] H. Fukuyama, Solid State Commun. **26**, 783 (1978).
[52] C. W. Rischau, S. Wiedmann, G. Seyfarth, D. LeBoeuf, K. Behnia, and B. Fauqué, Phys. Rev. B **95**, 085206 (2017).
[53] M. Zoraghi, J. Barzola-Quiquia, M. Stiller, P. D. Esquinazi, and I. Estrela-Lopis, Carbon **139**, 1074 (2018).